



32

33 **1. Introduction**

34 The Chinese Global operational Oceanography Forecasting System (CGOFS) running
35 at National Marine Environmental Forecasting Center of China (NMEFC) is used to
36 predict properties of global ocean, such as temperature, salinity, current, wave and sea
37 ice. The operational North-West Pacific Model (NWPM) is a regional model of
38 CGOFS consisting of a suite of nested model configurations, which produce daily
39 analysis and forecast, out to 5 days ahead, of the ocean variables, and provide the
40 nested configuration for East China Sea Model (ECSM) and South China Sea Model
41 (SCSM). The model component of NWPM is based on the Regional Ocean Model
42 System (ROMS) which is a free-surface, primitive equation ocean circulation model
43 formulated using terrain-following coordinates.

44 Model forecast requires the specification of initial conditions, and the accuracy of the
45 forecast depends on the accuracy of the initial conditions. Data assimilation is a
46 widely used and proved effective way to produce best estimates of the state of the
47 physical system by integrating observations into prognostic model. Over the past few
48 decades, many data assimilation methods have been developed for combining model
49 and observational data. These can broadly split into three approaches: Kalman Filter,
50 generally known as sequential schemes (Daley, 1991); Optimal Interpolation; and
51 variational methods (Lorenc, 1986), which are based on minimization of a cost
52 function that measures the differences between the model and the observations. The
53 Ensemble Kalman Filter (EnKF) was introduced by Evensen *et al.* (2003). Because of
54 the computational requirements limitation, the EnKF is not suitable for operational
55 forecasting system. As an approximation of EnKF, Ensemble Optimal Interpolation
56 (EnOI) scheme has been applied to ROMS to assimilate the along track Sea Level
57 Anomaly (TSLA) (Lv *et al.*, 2013). ROMS also is equipped with the four-dimensional
58 variational assimilation (4DVAR) method (Tshimanga *et al.*, 2008; Moore *et al.*, 2011a,
59 2011b), which isn't used in the operational forecasting system considering the
60 computational requirements. With considering the 3DVAR is the soundest path to the
61 ultimate development of more advanced data assimilation systems, Li *et al.* (2008) has



62 developed a 3DVAR approach for ROMS independently.
63 Three-dimensional variational (3DVAR) data assimilation method is a widely used
64 method in oceanic operational forecasting systems (e.g. Li et al, 2008). In this study
65 we applied an oceanographic three-dimensional variational data assimilation scheme
66 called OCEANVAR (Dobricic and Pinardi, 2008) to ROMS to assimilate the
67 Temperature and Salinity profiles from Argos. In order to illustrate and evaluate the
68 performance of the assimilation scheme, it was applied to the north-west pacific with
69 an eddy-resolving resolution. This system will be used in the future to augment the
70 quality of initial conditions for daily forecasts that has started to produce on
71 CGOFSv1.0.

72 The paper is organized as follows. The section 2 describes the components of the data
73 assimilation scheme for assimilating Argos profiles in the North-west Pacific. The
74 results from data assimilation are presented in the section 3, with focusing on the
75 performance of 3DVAR and multivariate properties. Finally, section 4 presents
76 conclusions.

77 **2. Model and data**

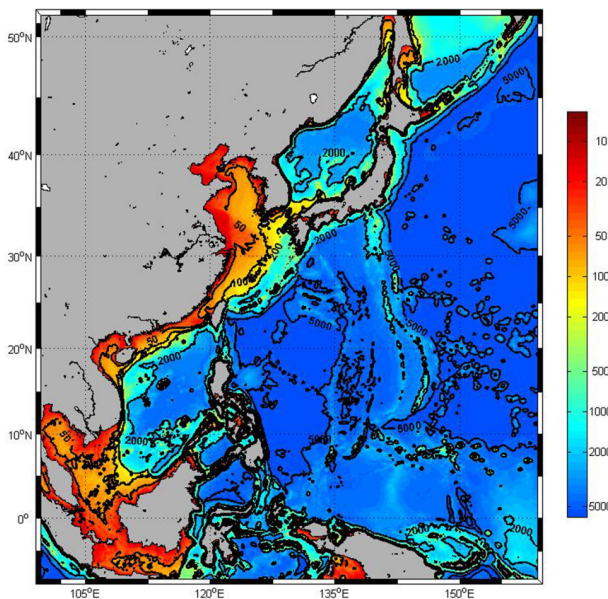
78 **2.1 model configuration**

79 The ROMS (Shchepetkin and McWilliams 2005; Malcolm et al., 2009) used in this
80 paper is a free-surface and primitive equation ocean circulation model formulated
81 using terrain-following coordinates, which is widely used in oceanic studies (Wang, et
82 al. 2012, Lv et al.,2014) . The model domain in this study is North-west Pacific Ocean
83 that extends from 8°S to 52°N and from 99°E to 160°E, as shown in Figure 2.1. The
84 horizontal resolution is 1/20° in both zonal and meridional directions with a total
85 horizontal grid points of 1098×1084 . In vertical, there are 30σ layers. The maximum
86 depth is set to 7000 m to keep the pattern stable. The bathymetry used here is derived
87 from GEBCO (General Bathymetric Chart of the Oceans), a global 30 arc-second
88 gridded bathymetry, which was supplied by the Intergovernmental Oceanographic
89 Commission and International Hydrographic Organization. To reduce the influence of
90 the seamount on model stability, the bathymetry is smoothed appropriately.
91 Considering the effects of an open boundary on simulation, southern, western and



92 northern boundaries are set as open boundaries, of which water level and velocity are
93 also obtained from SODA. The internal model time step is 300s and the external
94 model time step is 10s. The Yangtze River, Pearl River and Mekong River use
95 monthly mean runoff values in the model.

96 The model is spun-up for 10 years with the COADS (Comprehensive
97 Ocean-Atmosphere Data Set) monthly climatological mean air-sea flux to get an
98 initial state. From this initial condition, the model is forced by the NCEP/NCAR
99 Reanalysis2 4× daily data to simulate condition for the period of 1990-2005. The
100 initial conditions for both the control and the assimilation runs are provided by the
101 simulated ocean state at the end of 2005. In addition, the control test for 2006
102 without data assimilation provides a basis for comparison.



103
104 *Fig.2.1. Bathymetry of the North-west Pacific in the numerical model (depths in*
105 *meters)*

106 2.2. Assimilation algorithms

107 In recent years, progress in ocean data assimilation has been enabled along with the
108 advances in computing machinery and mathematical roots. The basic goal of the
109 ROMS 3DVAR system is to provide an “optimal” estimate of the true oceanic state at
110 analysis time through solving the assimilation problem by minimizing the prescribed



111 cost function (Ide et al. 1997)

$$\begin{aligned} \mathcal{J} &= \mathcal{J}_b + \mathcal{J}_o \\ &= \frac{1}{2}(x - x^b)^T \mathbf{B}^{-1}(x - x^b) + \frac{1}{2}[H(x) - y^o]^T \mathbf{R}^{-1}[H(x) - y^o] \end{aligned} \quad (2.1)$$

113 Where x is the unknown ocean state, equal to the analysis x^a at the minimum of \mathcal{J} ;
114 x^b is the background, which is an a priori estimate of the state of the ocean; y^o is the
115 vector of the observations; $y = H(x)$ is transform the gridded analysis x to
116 observation space, with H is the linear observation operator; and B and R are the
117 covariance matrices of the background and observational errors, respectively. The Eq.
118 (2.1) is linearized around the background state (e.g. Lorenc, 1997) into the following
119 form:

$$\mathcal{J} = \frac{1}{2}\delta x^T \mathbf{B}^{-1}\delta x + \frac{1}{2}(\mathbf{H}\delta x - d)^T \mathbf{R}^{-1}(\mathbf{H}\delta x - d) \quad (2.2)$$

121 Where $d = [y^o - H(x_b)]$ is the misfit, H is the linearized observations operator
122 evaluated at $x = x_b$ and $\delta x = x - x_b$ are the increments. The minimization problem
123 is defined on the field of increments in Eq. (2.2) which has a single minimum.

124 The 3DVAR system uses vertical Empirical Orthogonal Functions (v-EOFs) to
125 represent vertical modes of the background-error correlation matrix. The new v-EOFs
126 are considered time with monthly timescales.

127 The use of adjoint operations, which can be regarded as a multidimensional
128 application of the chain-rule for partial differentiation, permits efficient calculation of
129 the gradient of the cost function. The Quasi-Newton L-BFGS (Limited-memory
130 Broyden-Fletcher-Goldfarb-Shanno, Byrd et al., 1995) is used to efficiently combine
131 cost function, gradient and the analysis information to produce the “Optimal”
132 analysis.

133 The data assimilation systems, such as OI, EnKF, and 3DVAR, have led to improved
134 forecast scores relatively quickly. The practical advantages of VAR system over other
135 methods are listed below. Firstly, the VAR solution uses all observations
136 simultaneously, compared to the OI technique for which the process of data selection
137 into artificial sub-domains is required; secondly, synoptic data, such as satellite and
138 radar observations, can be assimilated near its validity time; Thirdly, balance, for



139 weak geostrophy and hydrostatic, constraints can be built into the preconditioning of
140 the coast function minimization. Even with such practical advantages, VAR system
141 still shows some weaknesses in real practice. Firstly, given both imperfect
142 observations and prior (e.g. background) information as inputs to the assimilation
143 system, the quality of the output analysis depends crucially on the accuracy of
144 prescribed errors. Secondly, although the variational method allows for the inclusion
145 of linearized dynamical/physical processes, in reality, real errors in the prediction
146 system may be highly nonlinear, which limits the usefulness of variational data
147 assimilation in highly nonlinear regimes, e.g. the convective scale or in the tropics.

148 **3. Model Validation**

149 In this section, we show the results of the assimilation of in situ data from January
150 2006 to March 2007. We discuss the validation of the analysis to evaluated the
151 performance of the assimilated model, wherein the simulated fields and the analysis
152 fields are called SF and AF, respectively.

153 **3.1. Consistency**

154 Consistency checks were carried out by comparing the AF monthly mean SST with
155 the Merged satellite and in situ data Global Daily Sea Surface Temperatures
156 (MGDSST).

157 Fig. 3.1 shows monthly mean average SST in January, April, July and October of
158 2006 from simulation and MGDSST respectively. The model SST (Fig. 3.1(b)) is
159 consistent with that derived from MGDSST (Fig. 3.1(a)). In subtropical basins,
160 temperature is generally high near the western boundary. While in sub-polar basins,
161 the zonal temperature gradient reverses sign, with low temperature in the western
162 basin. In addition, SST is reduced in pole-ward direction, with high temperature in the
163 equatorial Pacific and low temperature in the polar Pacific. Simulated SST is higher in
164 summer and lower in winter, compared to MGDSST (Fig. 3.1(d)). SST is generally
165 similar to the MGDSST in subtropical basins, meanwhile shows the pattern of high in
166 summer and low in winter, to the north of 40°N. The ocean model at high spatial
167 resolution can reasonably simulate the distribution of the warm pool.

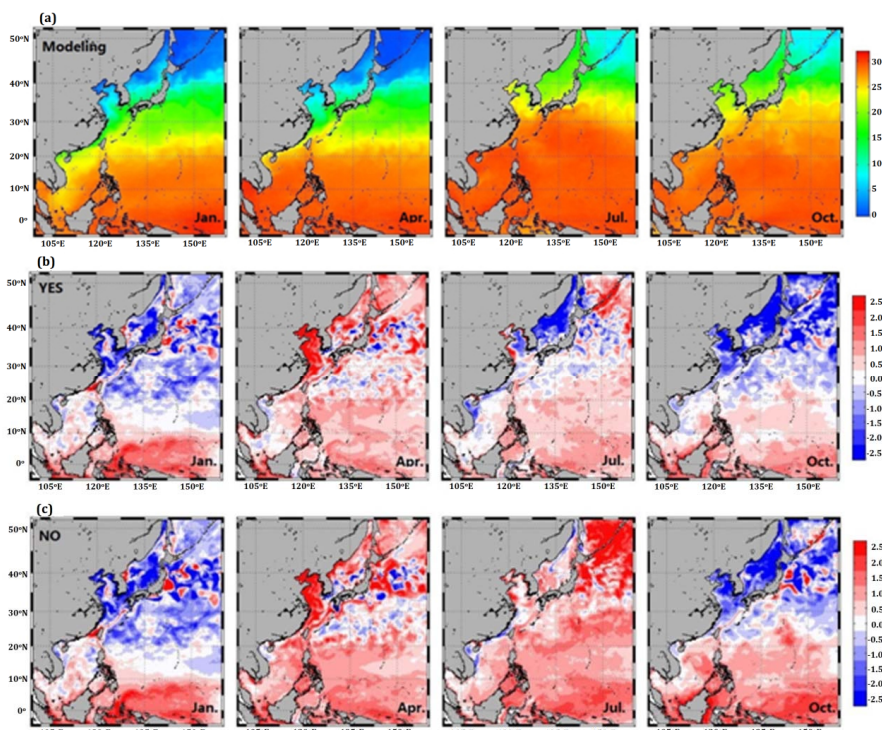
168 In order to understand the effect of data assimilation for temperature, Fig. 3.1(b) and



169 Fig. 3.1(c) show the differences between the observation and analysis or simulation,
170 respectively. First of all, the AF SST errors are generally smaller than the
171 corresponding SF, thus closer to the MGDSST observations. The SST has substantial
172 improvement in the South China Sea, the East China Sea and the Subtropics Pacific
173 after data assimilation. The SST error in Kuroshio Extension also has improvement in
174 the AF in agreement with the in-situ and satellite observations.

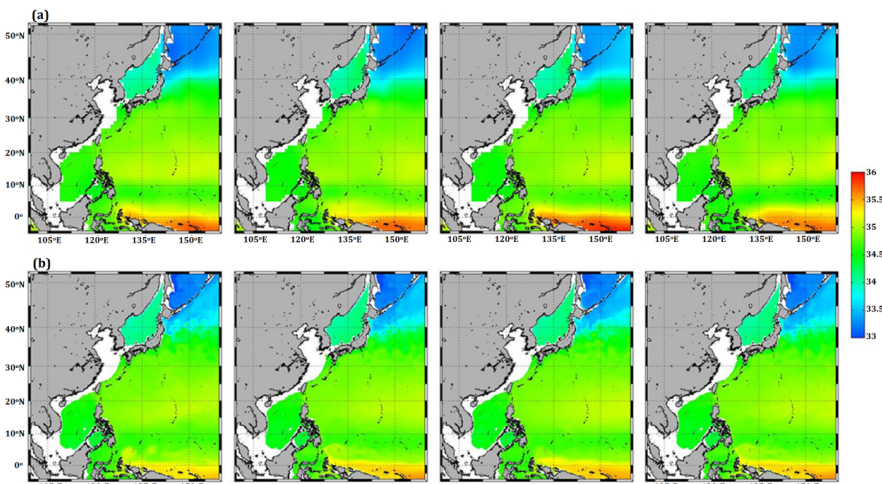
175 Fig. 3.2 shows the salinity profiles of simulations and observations, which are derived
176 from the EN4.0.2 dataset at 150 m ($1^\circ \times 1^\circ$, Good *et al.*, 2013). Although the AF
177 salinity for the tropic Pacific is less saline than the observation, the AF salinity for the
178 sub-tropic Pacific is very similar with the observation, which means that AF salinity
179 can catch main characteristics of actual salinity patterns.

180 Temperature section of 136°E is presented in Fig. 3.3, which shows some significant
181 qualitative differences. Fig. 3.3(b) shows the section with the AF and Fig 3.3(a) shows
182 the corresponding observation of EN4.0.2. Fig. 3.4(a) and Fig. 3.4(b) show the
183 salinity section with AF and EN4, respectively. The assimilation is capable of
184 modifying the vertical extension of Pacific.



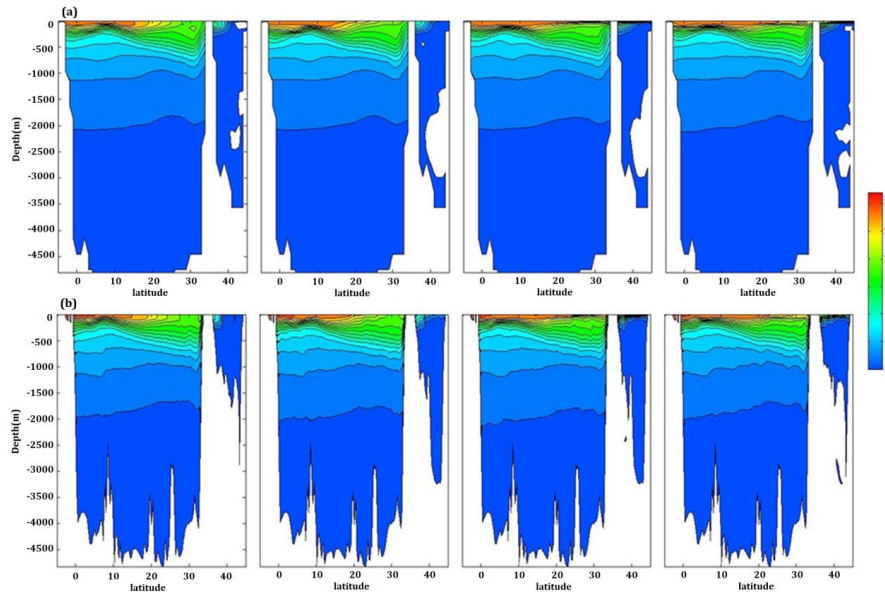
185

186 *Fig. 3.1. Monthly mean temperature at 150 m depth (°C) for January, April, July and October*
 187 *2006.(a)The SST of AF; (b)difference between MGDSST and AF; (c) difference between*
 188 *MGDSST and SF.*



189

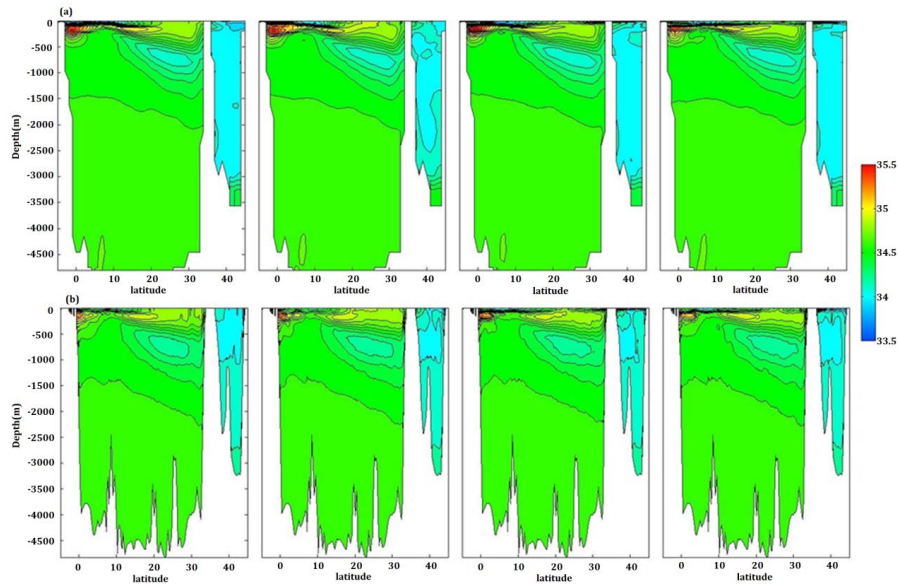
190 *Fig. 3.2. Monthly mean salinity at 150 m depth (in psu) in January, April, July and October*
 191 *2006.(a) EN4, (b) AF*



192

193

Fig. 3.3. Temperature (in °C) section of 136°E for (a) EN4 and (b) AF



194

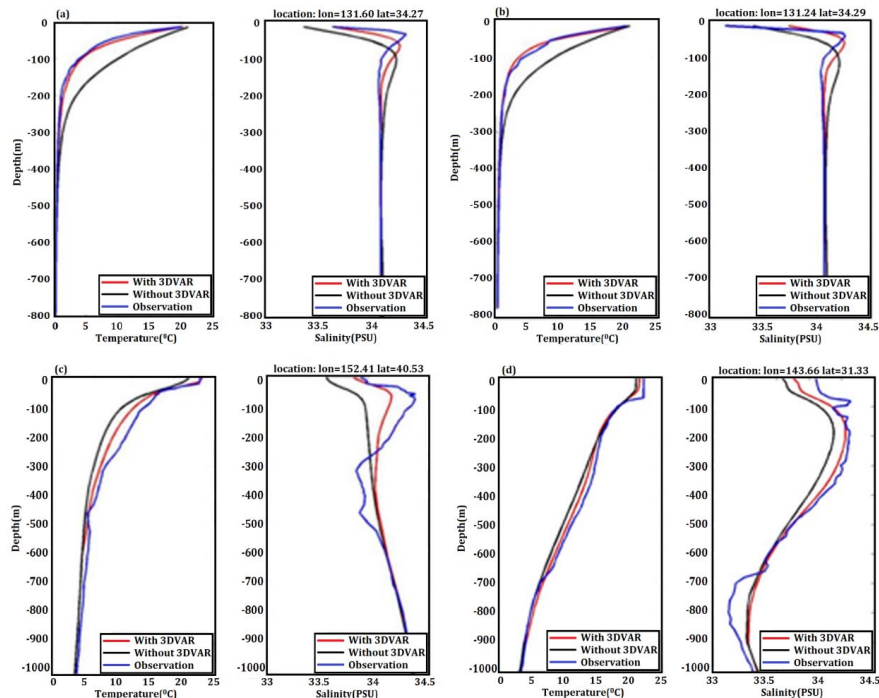
195

Fig. 3.4. Salinity (in psu) section of 136°E for (a) EN4 And (b) AF

196 Finally, a qualitative analysis of the impact of the assimilation in the modeling region
 197 is shown as follow. In Fig. 3.5(a), (b), (c), and (d), the differences in the study region
 198 of before and after assimilation profiles are shown together with the observed profiles.
 199 As shown, the profiles after assimilation are between the SF profiles and the



200 observations. The comparison results show that the data assimilation system is
 201 capable of correcting the model, with an effect of bringing the model closer to the
 202 observations.



203
 204 *Fig. 3.5. The vertical profiles for temperature (in °C) and salinity (in psu), where, red line*
 205 *stands for AF, black line stands for SF and blue line stands for observation; vertical and*
 206 *horizontal axes are depth (m) and temperature or salinity, respectively.*

207 3.2 Accuracy

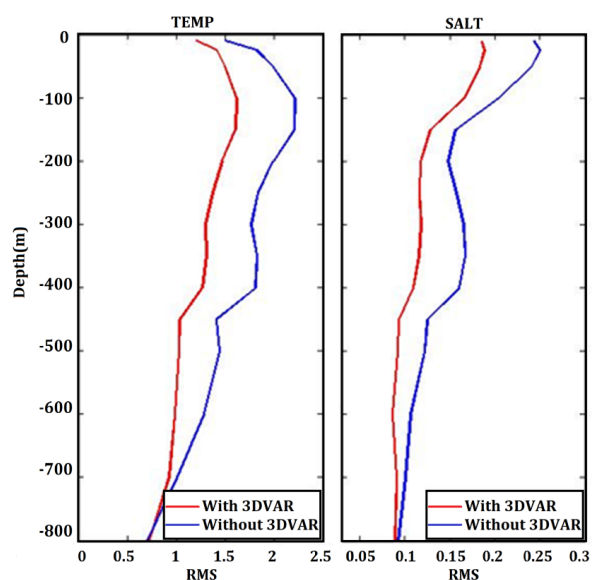
208 Some quantitative information on the analysis quality can be obtained by comparing
 209 the analyses with the observations at the observation locations. We use the misfit error
 210 which is the difference between the observation and the SF or AF to analyze the
 211 improvement of the model solution due to the regular data assimilation, although the
 212 data isn't independent. The Root Mean Square (RMS) between the SF or AF values
 213 and the observation values is defined as:

$$214 \quad \text{RMS} = \sqrt{\frac{1}{n} \sum_{i=1}^n (\varphi_m - \varphi_o)^2} \quad (3.1)$$

215 where, φ_m and φ_o stand for model and observation values of temperature or
 216 salinity respectively, n is the number of observation during the assimilation cycle.



217 Fig. 3.6 shows the RMS of temperature and salinity misfits which calculated as Argo
218 observation minus background value. The experiment with 3DVAR analyses has a
219 lower RMS of misfits than the experiment without assimilation. Furthermore, the
220 RMS with the assimilation becomes practically insignificant in deeper layer of the
221 ocean. As shown in the left panel of Fig. 3.6, the RMS of temperature misfits has the
222 maximum at ~100 m depth which approximately corresponds to the depth of the
223 mixed layer. The RMS of temperature misfits is relatively small close to the surface,
224 probably due to the fact that surface temperature is relaxed towards MGD SST
225 observations in both experiments. As shown in the right panel of Fig. 3.6, the RMS of
226 salinity misfits is significantly reduced after assimilation, especially at the depths
227 between ~200 m and ~400 m. However, the RMS of misfits increases towards the
228 surface in both experiments. The reason can be explained by the surface water and salt
229 flux, which is computed by relaxing the surface salinity towards climatology in the
230 model.



231

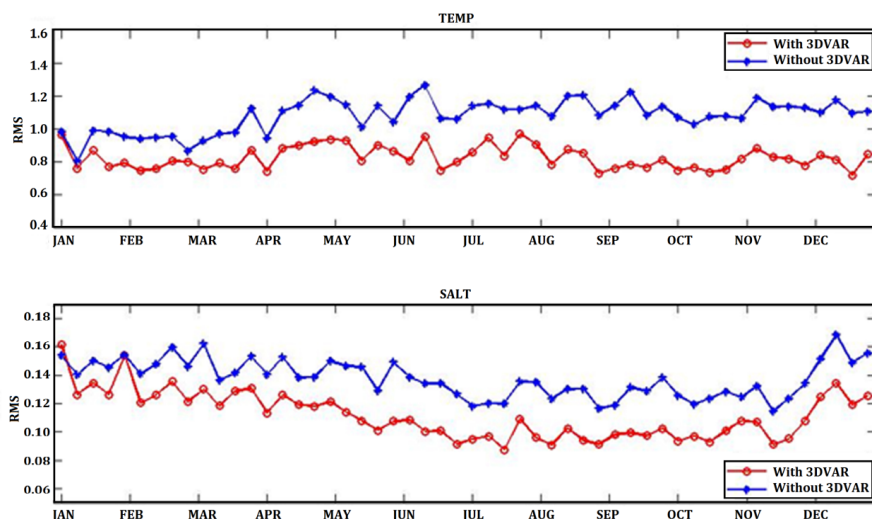
232 *Fig. 3.6. The vertical RMS for temperature (a) and salinity (b), where red line is the RMS of*
233 *misfits from AF, and blue line is the RMS of misfits from SF*

234 To show how the assimilation impacts the quality of temperature and salinity in the
235 North-west Pacific, the RMS differences between AF and SF for the 1-year



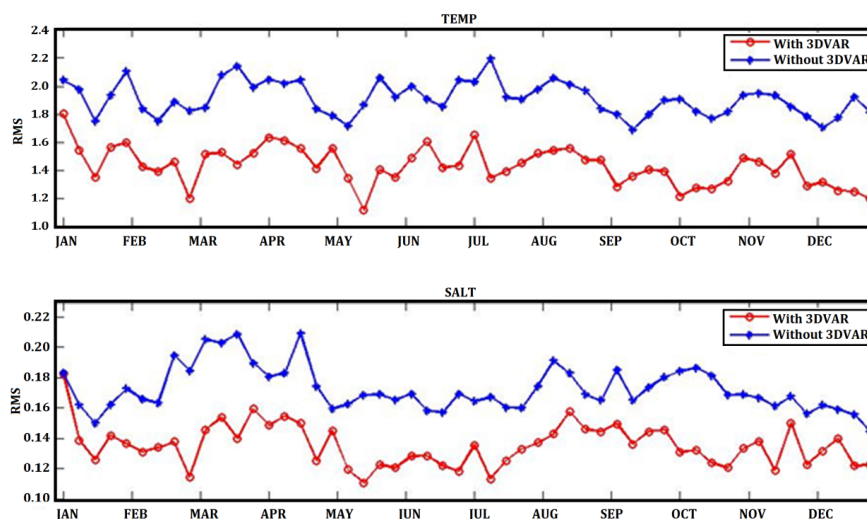
236 assimilation interval are displayed in Fig. 3.7 and 3.8. The statistics are divided into
237 two regions, the tropics (the south of 23.5°N, Fig. 3.7) and outside the tropics (the
238 north of 23.5°N, Fig. 3.8). The red line and blue line stand for the RMS of AF and SF
239 respectively in both figures .,

240 In the tropics, the AF performs better and better than the SF over time. As shown in
241 the upper panel of Fig. 3.7, the RMS of AF and SF temperature misfits approximately
242 fit the observation equally well, only with the AF slightly closer to the observation
243 data. The RMS of AF is ~ 0.83 °C in 2006, which is improved by $\sim 23.2\%$ compared
244 to ~ 1.08 °C of SF. As shown in the lower panel of Fig. 3.7, the RMS of AF salinity
245 misfits performs better than the RMS of SF, with ~ 0.112 (PSU) of AF compared to
246 ~ 0.138 (PSU) of SF.



247
248 *Fig. 3.7. The RMS misfits for temperature ((a), in °C) and salinity ((b), in psu) in tropic during*
249 *assimilation year (2006), where red line stands for RMS misfits with data assimilation and*
250 *blue line stands for RMS misfits without data assimilation.*

251 In the sub-tropic, the RMS of AF also performs a greater improvement than SF. As
252 shown in the upper panel of Fig. 3.8, the RMS of AF is ~ 1.43 °C in 2006, which is
253 improved by $\sim 25.1\%$ compared to ~ 1.91 °C of SF. As shown in the lower panel of
254 Fig. 3.8, the RMS of AF salinity misfits performs better than the RMS of SF, with
255 ~ 0.135 (PSU) of AF compared to ~ 0.173 (PSU) of SF, which is improved by $\sim 22.0\%$.



256
257 *Fig. 3.8. The RMS misfits for temperature ((a), in °C) and salinity ((b), in psu) in sub-tropic*
258 *during assimilation year (2006), where red line stand for RMS misfits with data assimilation*
259 *and blue line stand for RMS misfits without data assimilation.*

260 4. Summary

261 In this paper, we implement 3DVAR on ROMS with the ability to assimilate the T&S
262 Argos profiles. The data assimilation system is tested on an eddy-resolving model of
263 the North-west Pacific. A specific feature of ROMS 3DVAR system is separating the
264 background error covariance matrix into vertical and horizontal modes in order to
265 reduce the order of the data assimilation. Horizontal covariance is modeled as
266 Gaussian function, whilst vertical covariance which is calculated from a long-term
267 model simulation is represented by Empirical Orthogonal Functions (EOFs).

268 The T&S of Argos profiles are assimilated into the North-west Pacific model for the
269 period of 2006. Results show that the assimilation system can get a beneficial effect in
270 the model region.

271 The analysis produced by the data assimilation has been validated by the monthly
272 means SST from satellite, which is an independent observation. In the model region,
273 the data assimilation system has the capability of “bringing” the model closer to the
274 observations.

275 Statistical indexes indicate that the RMS of misfits for temperature is less than 1.0 °C
276 in the tropics domain and less than 1.5 °C in the subtropics domain with the main



277 error from the Kuroshio Extension region. The RMS misfit salinity error is less than
278 0.15 PSU in the model region.

279 **Acknowledgments**

280 *This work was supported by The National Natural Science Foundation of China under contract No.*
281 *41222038, 41206023 ; the National Basic Research Program of China (“973” Program) under*
282 *contract No. 2011CB403606; and the “Strategic Priority Research Program” of the Chinese Academy*
283 *of Sciences Grant No. XDA1102010403.*

284 **References**

- 285 Byrd, R.H., Lu, P., Nocedal, J., Zhu, C., 1995: A limited memory algorithm for bound constrained
286 optimization. *SIAM Journal on Scientific Computing* 16, 1190–1208.
- 287 DALEY, R. 1991: *Atmospheric data Analysis*, Cambridge University Press, Cambridge U. K., p 471.
- 288 Dobricic S., Pinardi N., 2008: An oceanographic three-dimensional variational data assimilation scheme.
289 *Ocean Modelling* 22, 89–105
- 290 Good, S. A., M. J. Martin and N. A. Rayner, 2013. EN4: quality controlled ocean temperature and
291 salinity profiles and monthly objective analyses with uncertainty estimates, *Journal of Geophysical*
292 *Research: Oceans*, 118, 6704-6716, doi:10.1002/2013JC009067
- 293 Ide, K., P. Courtier, M. Ghil, and A. C. Lorenc, 1997: Unified notation for data assimilation:
294 Operational, sequential and variational. *J. Met. Soc. Japan*, 75, 181-189.
- 295 Li Z., Chao Y., McWilliams J.C and Ide K., 2008.: A three-dimensional variational data assimilation
296 scheme for the regional ocean modeling system. *J. Atmos. Ocean. Tech.*, 25, 2074-2090
- 297 Lorenc, A. C., 1986: Analysis methods for numerical weather prediction. *Quart. J. Roy. Meteor. Soc.*,
298 112, 1177-1194.
- 299 Lorenc, A.C., 1997: Development of an operational variational assimilation scheme. *Journal of the*
300 *Meteorological Society of Japan* 75, 339–346.
- 301 Lv G.K, Wang H., Zhu J. et al. 2014: Assimilating the along-track sea level anomaly into the regional
302 ocean modeling system using the ensemble optimal interpolation. *Acta Oceanologica Sinica*. Vol. 33,
303 Issue7, 72-82
- 304 Moore, A.M., et al., 2011a: The Regional Ocean Modeling System (ROMS) 4-dimensional variational
305 data assimilation systems Part I – System overview and formulation. *Prog. Oceanogr.* 91. 34–49.
- 306 Moore, A.M., et al., 2011b: The Regional Ocean Modeling System (ROMS) 4-dimensional variational



- 307 data assimilation systems. *Prog. Oceanogr.* doi:10.1016/j.pocean.2011.05.003
- 308 Malcolm J, Roberts A, Clayton M, et al., 2009: Impact of resolution on the Tropical Circulation in a
309 matrix of coupled models. *J Clim*, 22:2541-2556
- 310 Schepetkin, A.F., and McWilliams J.C., 2003: A method for computing horizontal pressure-gradient
311 force in an oceanic model with a nonaligned vertical coordinate. *J. Geophys. Res.*, 108, 3090,
312 doi:10.1029/2001JC001047
- 313 Schepetkin, A.F., and McWilliams J.C., 2005: The regional ocean modeling system (ROMS): A
314 split-explicit, free-surface, topography-following-coordinate oceanic model. *Ocean Modell.*, 9, 347-404
- 315 Tshimanga, J., S. Gratton, A.T. Weaver and A. Sartenaer, 2008: Limited-memory preconditioners with
316 application to incremental variational data assimilation. *Q. J. R. Meteorol. Soc.*, 134, 751-769.
- 317 Wang H., Wang Z.Y., Zhu X.M., Wang D.K. and Liu G.M., 2012: Numerical study and prediction of
318 nuclear contaminant transport from Fukushima Daiichi nuclear power plant in the North Pacific Ocean.
319 *Chin. Sci. Bull.*, Vol.57, No.26:3518-3524